

Separating repeating fast radio bursts using the minimum spanning tree as an unsupervised methodology

C. R. GARCÍA,^{1,2} DIEGO F. TORRES,^{1,3,2} JIA-MING ZHU-GE,^{4,5} AND BING ZHANG^{4,5}

¹*Institute of Space Sciences (ICE, CSIC), Campus UAB, Carrer de Can Magrans s/n, 08193 Barcelona, Spain*

²*Institut d'Estudis Espacials de Catalunya (IEEC), 08034 Barcelona, Spain*

³*Institució Catalana de Recerca i Estudis Avançats (ICREA), E-08010 Barcelona, Spain*

⁴*Nevada Center for Astrophysics, University of Nevada, Las Vegas, NV 89154, USA*

⁵*Department of Physics and Astronomy, University of Nevada, Las Vegas, NV 89154, USA*

ABSTRACT

Fast radio bursts (FRBs) represent one of the most intriguing phenomena in modern astrophysics. However, their classification into repeaters and non-repeaters is challenging. Here, we present the application of the graph theory Minimum Spanning Tree (MST) methodology as an unsupervised classifier of repeaters and non-repeaters FRBs. By constructing MSTs based on various combinations of variables, we identify those that lead to MSTs that exhibit a localized high density of repeaters at each side of the node with the largest betweenness centrality. Comparing the separation power of this methodology against known machine learning methods, and with the random expectation results, we assess the efficiency of the MST-based approach to unravel the physical implications behind the graph pattern. We finally propose a list of potential repeater candidates derived from the analysis using the MST.

Keywords: transients: fast radio bursts - methods: data analysis

1. INTRODUCTION

Fast Radio Bursts (FRBs), first detected in 2001 by the Parkes Telescope and reported in 2007 (Lorimer et al. 2007), are transient radio pulses, typically in millisecond timescales and originating from cosmological distances. FRBs have attracted considerable interest and numerous physical interpretations; see, e.g., Katz (2018); Popov et al. (2018); Cordes & Chatterjee (2019); Petroff et al. (2019); Platts et al. (2019); Zhang (2020); Xiao et al. (2021); Petroff et al. (2022); Xiao et al. (2022); Zhang (2023). The observed properties of FRBs, such as their dispersion (DM) and rotation (RM) measure, provide clues into the physical characteristics of the intervening medium, including density and magnetic field strength. Their energy or brightness temperature also offers valuable hints regarding the underlying mechanisms driving the FRB emission. It has been proposed that their emission could be powered by the dissipation of magnetic fields of a magnetar (Popov & Postnov 2013; Lyubarsky 2014; Katz 2016; Lu & Kumar 2016; Murase et al. 2016; Kumar et al. 2017; Nicholl et al. 2017; Margalit & Metzger 2018; Lu et al. 2020; Yang & Zhang 2021).

This has been substantiated after the Canadian Hydrogen Intensity Mapping Experiment (CHIME) (CHIME/FRB Collaboration et al. 2020) and STARE-2 (Bochenek et al. 2020) discovered FRB 200428 in association with a hard X-ray burst from the Galactic magnetar, SGR 1935+2154 (Li et al. 2021; Mereghetti et al. 2020).

After the discovery of the first repeater in 2016, FRB 20121102A (Spitler et al. 2016; Scholz et al. 2016), FRBs are broadly categorized into two groups based on their repetition properties: repeaters and (apparently) non-repeaters. In the magnetar interpretation, such differences may arise from age, with young magnetars producing a higher repetition rate than older ones, see e.g., Beloborodov (2017); Metzger et al. (2017); Feng et al. (2022).

However, synthesizing the physical causes behind these differences and escaping from often not fully understood observational biases remains a significant challenge.

Here, we aim to explore a novel classification tool for FRBs, separating them into repeaters and non-repeaters (for other approaches, see, e.g., Palaniswamy et al. (2018); Caleb et al. (2019); Ai et al. (2021); Luo et al. (2023); Zhu-Ge et al. (2023)). We shall use graph theory (e.g., Wilson (2010)) and principal component anal-

ysis (PCA, e.g., [Pearson \(1901\)](#); [Shlens \(2014\)](#)). Graph theory aims to establish relationships between objects based on their connections and represent them in a graph. In particular, we introduce a graph called the minimum spanning tree (MST, see recent astrophysical applications in [García et al. \(2022\)](#); [García & Torres \(2023\)](#); [Vohl et al. \(2023\)](#)) as an unsupervised learning approach with a supervised evaluation. The MST, where each node will represent an FRB, provides a manageable and compact structure calculated in an N -dimensional space. Aided by the fundamental properties on which the MST is built, we will explore its capacity to establish the variables that show the best separation power and then indicate a group of likely repeating FRBs that have not yet been classified as such. Using an unsupervised learning approach is particularly appealing when one does not control which properties within a data set are driving a classification, as is the case here. In addition, even the labels themselves are subject to possible change in time, as non-repeaters could become repeaters. Also, such methods do not necessarily require sample splitting for proper application. This is valuable since the sample is not large and contains at most 750 FRBs, so we are not in the realm of big data. Randomly cutting the sample, in a training set (say, 80%/20% in size), would imply that 150 FRBs are sufficient to test the pattern behind a repeater/non-repeater classification, which we consider a risk. Finally, the MST as an unsupervised method offers transparency in indicating the importance of the variables that best separate repeaters from non-repeaters. This becomes less clear in supervised methods when techniques such as feature importance (see eg., [Breiman \(2001\)](#); [Altmann et al. \(2010\)](#); [Casalicchio et al. \(2018\)](#); [Fisher et al. \(2018\)](#)) or Shapley Additive exPlanations (SHAP, see [Lundberg & Lee \(2017\)](#); [Lundberg et al. \(2018\)](#) for more details) are applied for that purpose.

2. SAMPLE, VARIABLES, PCA, AND MST

We use the sample from the Canadian Hydrogen Intensity Mapping Experiment Fast Radio Burst (CHIME/FRB) catalog ([CHIME/FRB Collaboration et al. 2021](#); [The Chime/FRB Collaboration et al. 2023](#)). We consider their 750 FRBs, with 265 as repeaters and 485 as non-repeaters. The group of repeaters corresponds to events coming from 70 localizations, and each FRB is taken individually as different events labeled as a repeater (as done in the CHIME catalog). Following the CHIME catalog, sub-bursts can be ascribed to both repeaters and non-repeaters, and they are also considered individual bursts, each with the correspond-

ing label. We exclude those six FRBs that have neither flux nor fluence measured.

To characterize an FRB we shall consider the logarithm of the following variables, (this is done just for convenience, as their values may differ by several orders of magnitude for different FRBs), including the ones that are directly measured ([CHIME/FRB Collaboration et al. 2021](#); [The Chime/FRB Collaboration et al. 2023](#)) such as peak frequency ν_c (MHz), flux S_ν (Jy), fluence F_ν (Jy ms), boxcar width Δt_{BC} (ms), and also derived parameters based on the DM- z relation (as presented in [Macquart et al. 2020](#); [Deng & Zhang 2014](#); [Luo et al. 2023](#); [Zhu-Ge et al. 2023](#)) such as redshift z , rest-frame frequency width $\Delta\nu$ (MHz), rest-frame width Δt_r (ms), burst energy E (erg), luminosity L (erg/s), and brightness temperature T_B (K). As their distribution is not normal (nor is it that of the original variables without logarithm), we use the robust scaler to scale them (i.e., we subtract the median and divide by the interquartile range, see, e.g., [de Amorim et al. \(2023\)](#))

$$x_i^\dagger = \frac{x_i - Q_2}{IQR}, \quad (1)$$

In Eq. (1) the \dagger -symbol represents that the quantity x_i has been scaled, Q_1 , Q_2 and Q_3 represent the 1st quartile, median, and 3rd quartile of the distribution, respectively, and IQR is the interquartile range, ($Q_3 - Q_1$).

As we can observe with the cross-correlations shown in [Fig. 1](#), the physical properties have a different classification power.

This can be corroborated by applying a simple separation method: for each of the magnitudes considered, we note the median of each distribution and count the number of repeaters positioned on each side of this central location. The best separation is provided by the rest-frame frequency width, which yields to 217 (82%) grouped FRB repeaters (all with a width lower than 397.24 MHz). This is far off from the random expectation: After producing 10^5 simulations in which repeater labels are randomly assigned, the average separation achieved is 52%, that is, a separation consistent with a fully random process in which labels are separated in equal numbers on both sides of the median. This high separation power of the rest-frame frequency width will serve as a threshold to validate the performance of other algorithms or classifiers. We shall look below for classifiers that will perform better than 82% in separating repeaters from non-repeaters.

[Figure 2](#) presents the outcome of conducting PCA over the logarithm of all the variables defined in this section. The left panel of [Fig. 2](#), also called the scree plot,



Figure 1. Cross-correlation of the logarithm of the 10 magnitudes considered. Repeaters (in blue) and non-repeaters (in red) are separately noted. The main diagonal shows the distribution for each variable.

shows the explained variance of each PC according to the eigenvalues of the covariance matrix. Note that the covariance matrix calculates the relationships between pairs of variables, showing how changes in one variable are associated with changes in another. It represents the amount of information contained in each PC. The central panel shows the cumulative explained variance of the PCs indicating how much of the total variance

is captured as more PCs are included. The right panel shows the ‘weight’, also called loading, that each variable has concerning each PC, indicating its contribution to the variance captured by that PC. These values correspond to the coefficients of the eigenvectors of the covariance matrix. Negative values imply that the variable and the PC are negatively correlated. In contrast, a positive value shows a positive correlation between the

PC and the variable. While the first six PCs contain the majority of variance, retaining over 99% of its informational content, the first three PCs contain 87% of it. Full variance coverage needs nine PCs, so the dimensionality reduction is not extreme if it is to be entirely retained. Thus, both the number of PCs needed to cover the total variance and the relative flat distribution of the loadings of the first PCs render its use a priori unappealing.

Expanding and formalizing the work by Kruskal (1956), Kleinberg & Tardos (2005); Erickson (2019) provide the foundational knowledge required to calculate the MST. Considering the MST as a graph that connects points in a N -dimensional, each point (or node) is connected to at least one other end by an edge whose length is associated with a given distance. The edges of an MST are chosen so that the sum of their lengths is minimal and all nodes are connected. Our previous studies García et al. (2022); García & Torres (2023), also Vohl et al. (2023), serve as a close example, as they discuss how these concepts are applied to a pulsar dataset. Here, we shall introduce the Euclidean distance (d), which is calculated considering the straight-line distance between two nodes (n, m) in a N -dimensional space following the next expression

$$d_{nm} = \sqrt{\sum_{j=1}^N (n_j - m_j)^2} . \quad (2)$$

The N -distance seen in Eq. (2), where N represents the set of variables considered, can be computed using all or part of the defined physical variables mentioned above or the PCs (employing the PCs that account for 100% of the explained variance yields an MST that is identical to the one derived using all magnitudes). Taking the Eq. (2), we initially generate a complete, undirected, weighted graph $G(V, E)$, characterized by a set V of nodes (each of them is an FRB) with a size of $|V|^1$ and set E of edges of size $|E|$. The latter values are assigned to a specific weight w equal to the Euclidean distance between the two FRBs, using all or part of the variables or PCs, as described. For each combination of variables, then, we will start from the graph $G(750, 280875)$ and derive an MST, $T(750, 749)$. To do this, we apply the called Kruskal’s algorithm (see eg., Kruskal (1956)), which connects the whole sample considering the minimum distance between them at a local state, looking for a global minimization as the final condition (see the references above for a more detailed explanation and examples).

¹ The notation $|\cdot|$ represents the cardinality (or size) of the specified set, indicating the number of elements within it.

3. ALGORITHM AND RESULTS

The total number of combinations (without repetition) from a set of 10 variables is $\sum_1^{10} \binom{10}{k} = 2^{10} - 1 = 1023$, reflecting the number of MSTs we compute. For each of these MSTs, we identify the node with the highest centrality of the graph through the betweenness centrality estimator (see Freeman (1977); Moxley & Moxley (1974); Brandes (2001); Baron & Ménard (2021)). This estimator identifies how often a particular node appears on the shortest path between any two other nodes, effectively measuring the node’s importance in terms of connectivity within the MST (see García & Torres (2023) and references therein for more details). Eliminating this node would separate T into several connected parts (or branches). The branch with the highest number of repeaters will be named the repeater branch. All other branches will be considered as non-repeater branches. A high density of repeaters in the repeater branch would qualify the variables under which the underlying Euclidean distance is built as a well-separated filter via the MST algorithm. To judge the performance of each MST seen as a classifier, we use the metrics: precision, recall, F_1 , and F_2 score plus the area under the curve (AUC or ROC-AUC). Precision measures the ratio of correctly identified repeaters regarding the total of FRBs (both repeaters and non-repeaters) of the repeater branch. At the same time, recall assesses the proportion of actual repeaters that are correctly identified. The F_1 score balances precision and recall equally, whereas the F_2 score places more emphasis on recall. AUC evaluates the overall discrimination ability of the classifier (see eg., Han et al. (2012) and the Appendix for more detailed definitions). In identifying high-density locations of repeaters, metrics such as recall and precision focus on correctly identifying actual repeaters and minimizing non-repeaters taken as repeaters. A high F_1 score indicates a good balance between recall and precision. On the other hand, the F_2 score, as seen, places more emphasis on recall than precision, effectively tolerating a certain level of misclassification of non-repeaters as repeaters. Lastly, a high AUC suggests that MST predictions rank true repeater instances higher than non-repeaters, which is crucial for identifying a high amount of repeaters among the whole sample. To determine the best combination of variables, we look for a combination that offers a balanced trade-off between precision and recall (as reflected in the F_1 Score) and considers the F_2 Score (which weighs recall higher than precision) and the ROC-AUC value for overall performance. This is in practice implemented by an overall rank (see, e.g., Li et al. (2017)), which averages all ranks across these evaluating metrics.

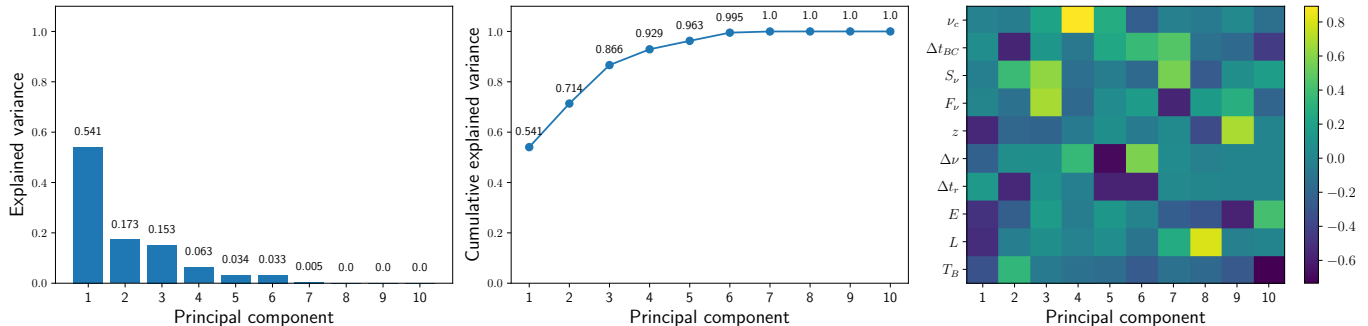


Figure 2. PCA results for the logarithm of the set of variables defined. Left panel: The scree plot shows the explained variance of each PC. Central panel: The cumulative explained variance of the PCs. Right panel: The loadings of each variable regarding the PCs. See the main text for further explanation.

Armed with the MST/betweenness centrality methodology and with the rankings we find that there are 25 combinations of variables, and 3 combinations of PCs, for which we obtain a separating, i.e., recall, better than 82%. Results are shown in Table 1. Recall values are notably high across the board, which is excellent if the primary concern is to minimize missing repeaters. The precision is lower in some combinations than recall, which is expected in a scenario where the recall is prioritized. The F_1 scores are still reasonably good, indicating a balanced performance between precision and recall. The F_2 scores are also high, reinforcing the model orientation towards recall which is desirable in contexts where the consequences of missing repeaters outweigh those of non-repeaters seen as repeaters. The ROC-AUC values are also far from what could be considered a random guess, showing a good degree of separability. Based on the overall rank, a combination of peak frequency, rest-frame frequency width, and brightness temperature (#1) achieves the best balance. Although this is not the best combination in terms of recall, for which it shows 0.8528, it is not far away from the best 0.8604 (a difference of just 2 repeaters) obtained with the combination (#7). Also, it shows a precision of 0.5825, being the second highest, which together with the aforementioned recall makes it the combination with the best F_1 score, F_2 score, and ROC value.

The results obtained using the PCs are also shown in Table 1. Recalling that we need 9 PCs to define the full variance, we consider $\sum_1^9 \binom{9}{k} = 2^9 - 1 = 511$. Only three combinations of PCs present results exceeding the threshold taken for recall, although they are not particularly more informative or ranked better than those obtained via the direct use of physical variables.

We observe consistently high recall rates exceeding around 0.82 across all combinations, highlighting their effectiveness in accurately identifying repeaters. The precision values, ranging approximately from 0.51 to

0.55, and corresponding F_1 scores between 0.63 to 0.67, suggest a reasonable balance between the accuracy of robust predictions and the method’s ability to identify actual repeaters. Furthermore, the F_2 scores, centered around 0.75, emphasize the evaluation’s focus on recall over precision, aligning with our classification goal to reduce misclassified repeaters. The ROC-AUC values, approximately 0.65 to 0.68, demonstrate the MST based on PCs’ robust capability to distinguish between repeaters and non-repeaters, indicating significant discriminative power. Additionally, the high Z-scores of 10 and 12 across the combinations underscore the statistical significance of these results, affirming that the observed recall rates are not due to chance. Taking into account these points through the overall rank, the combination (PC1, PC2, PC3) emerges as the most effective. This represents 87% of the total variance and has the best-separating power of all those using principal components. Having more variance described, with more PCs, does not yield a better separation power, implying that something else, other than the variables used to describe the sample here likely plays a role in the separation.

As before, we test the randomness of the process in two ways. First, we question whether, in case there is no link at all between repeating/non-repeating labels and the variables, we could still find a group of 25 combinations out of 1023 possible ones that could lead to a separating power over 82%. We do so by randomly relabelling the FRBs in repeaters and non-repeaters, maintaining the sample proportions, and building 10^5 fake samples for each MST using the same variables as the original.

We find that no combination of variables out of possible 1023 exceeds the threshold of 82% separating in any of the simulations performed. Second, for each combination selected in Table 1 we compare the real result (i.e., its real separation power) with the average of the recall of the fake samples, using the Z-score, a statisti-

cal measure that quantifies how many standard deviations a data point (in this case, the recall) is from the mean of the distribution (see e.g., Bruce et al. (2020) and the Appendix for more details). Table 1 shows that Z-scores obtained are at 9σ or higher for recall values, along all combinations, compared to distributions from fake sets. These randomness tests are a strong indicator of the effectiveness and robustness of this classification approach. In particular, the randomness of the best-ranked combination of variables, viewed in the Z-score of the first row in Table 1, is one of the lowest which proves a robust classification.

Combination #1 successfully identified a significant number of repeaters (226/265), ensuring that relatively few repeaters are missed (39/265). Some non-repeaters are located in the repeater branch of the MST (162/485). If there is any physical link between the variables and the repeating property, some of these should be candidates to appear as repeaters in the next catalog. We come back to this below. Fig. 3 shows the MST with the arrangement of repeaters and non-repeaters of combination #1, it separates the two types of FRBs.

3.1. Results considering selection effects

As explained in CHIME/FRB Collaboration et al. (2021), assessing selection effects is a challenge to be addressed in the study of FRBs. We have approached this question following the considerations in Section 3.3 of The Chime/FRB Collaboration et al. (2023). The following cuts in the sample have been imposed

1. Events measured by the *bonsai* real-time detection pipeline $S/N < 12$ are excluded due to being more likely misclassified as noise.
2. Events with $DM < 1.5 \max(DM_{NE2001}, DM_{YMW16})$ are excluded to minimize the possibility of having a wrong identification of rotating radio transients or radio pulsars as FRBs considering that a $\sim 50\%$ errors may be common in models used to estimate the Galactic DM.
3. Events detected in the telescope’s sidelobes (see Lin et al. (2023a,b)) are excluded since the understanding of the primary beam shape at large zenith angles is limited. This makes it difficult to characterize events.

We are left with 459 FRBs after considering such cuts. This is a significant reduction from the earlier sample (by about 40%). In this sample, we find 135 FRBs classified as repeaters. For each of the variables considered, again, we note the median of each distribution and count the number of repeaters positioned on each

side of this central location. The best classification is provided once again for this reduced sample by the rest-frame frequency width, which can separate 109 of the 135 repeaters (80%). Thus, we test whether our methodology provides a separating power that goes beyond this threshold. After applying it similarly to what has been done for the full sample we find 15 different combinations of variables for which the separating performance exceeds the one provided by the rest-frame frequency width.

We note two aspects of interest, selection effects may indeed play a role both forcing to work with reduced samples whose properties are likely not well mapped yet due to low-number statistics, and changing the total variance. As a result, the PCA analysis and the combination of variables for which the separating power is high are different when compared with those corresponding to the full sample. However, it can be recognized that peak frequency, rest-frame frequency width, and brightness temperature (variables in #1, see Table 1) are among the variables that appear the most in all combinations with large separating power, whereas, on the other hand, the burst energy is the least implied, offering little classification power.

4. CONCLUSIONS

To our knowledge, this is the first application of the graph theory MST technique to separate the repetition properties of FRBs. To some extent, this work relates to that of Bhatporia et al. (2023) when using mathematical techniques to classify the population of the FRBs, although in their case performance metrics are not provided. Our performance metrics indicate that the MST classifiers do a good job of separating repeaters among the FRBs, excelling especially in recall and thus minimizing false negatives. This approach demonstrates the potential for practical application and can contribute to the scientific understanding of FRBs by highlighting the importance of certain variables over others concerning what best describes the repetitive character of a source. Methodologically, we are not defining clusters over the MST, we compute instead the betweenness centrality for each node and identify the one with the highest value (the black node in Fig. 3). This node acts as a bridge within the MST, by removing it, we partition the graph into separate branches. We then use the labels to count the number of repeaters on each branch, which allows us to study the distribution of repeaters and non-repeaters. Since we do not cluster, we do not confront such issues as chaining or unbalanced clustering seen, for example, in single linkage algorithms (see Everitt et al. (2011) for a discussion). Importantly, we do not use the labels

Table 1. Summary of performance metrics of the combination of variables selected as those exceeding the threshold of 0.82 recall is seen in the rest-frame frequency width, sorted by overall rank. The combinations seen in the ‘variables’ column are named as follows: (1): $\log\nu_c$, (2): $\log\Delta t_{BC}$, (3): $\log S_\nu$, (4): $\log F_\nu$, (5): $\log z$, (6): $\log\Delta\nu$, (7): $\log\Delta t_r$, (8): $\log E$, (9): $\log L$, and (10): $\log T_B$.

#	Variables	Precision	Recall	F_1 Score	F_2 Score	ROC-AUC	Z Score
1	[1, 6, 10]	0.5825	0.8528	0.6922	0.7804	0.7773	14
2	[1, 5, 6, 7]	0.5622	0.8528	0.6777	0.7729	0.7033	13
3	[1, 2, 5, 6, 10]	0.5589	0.8415	0.6717	0.7642	0.7285	13
4	[1, 3, 4, 6, 7, 8, 9, 10]	0.5784	0.8491	0.6881	0.7764	0.6834	13
5	[1, 5, 6, 8, 10]	0.5878	0.8340	0.6895	0.7695	0.6961	14
6	[6]	0.5722	0.8226	0.6749	0.7564	0.7522	19
7	[1, 2, 3, 6, 7, 8]	0.5352	0.8604	0.6599	0.7672	0.6941	12
8	[1, 3, 5, 6, 9]	0.5510	0.8566	0.6706	0.7711	0.6577	13
9	[1, 2, 3, 4, 6, 7, 9, 10]	0.5457	0.8340	0.6597	0.7543	0.7007	12
10	[2, 5, 10]	0.5598	0.8302	0.6687	0.7571	0.6999	13
11	[1, 3, 5, 6]	0.5509	0.8377	0.6647	0.7587	0.6645	12
12	[1, 4, 5, 6, 9]	0.5688	0.8264	0.6738	0.7578	0.6583	13
13	[5, 6, 9, 10]	0.5198	0.8415	0.6427	0.7488	0.6883	11
14	[8, 10]	0.5298	0.8377	0.6491	0.7505	0.6859	11
15	[2, 6, 8]	0.5366	0.8302	0.6519	0.7483	0.7006	12
16	[1, 2, 4, 6, 7, 9, 10]	0.5239	0.8264	0.6413	0.7409	0.7230	11
17	[1, 2, 4, 5, 6, 10]	0.5201	0.8302	0.6395	0.7417	0.7118	11
18	[1, 4, 6, 9, 10]	0.5116	0.8302	0.6331	0.7383	0.7013	10
19	[1, 2, 3, 6, 9, 10]	0.5117	0.8226	0.6310	0.7335	0.7180	10
20	[1, 2, 4, 5, 6, 9, 10]	0.5034	0.8302	0.6268	0.7348	0.7002	10
21	[1, 2, 3, 4, 6, 7, 8, 9]	0.4966	0.8377	0.6236	0.7366	0.6590	10
22	[1, 2, 4, 5, 6]	0.4944	0.8340	0.6208	0.7332	0.6866	10
23	[1, 6, 8, 9, 10]	0.4846	0.8302	0.6120	0.7266	0.7026	9
24	[1, 5, 6, 9, 10]	0.4944	0.8302	0.6197	0.7309	0.6987	10
25	[1, 4, 5, 6, 9, 10]	0.4943	0.8226	0.6176	0.7262	0.6851	10
1	[PC1,PC2,PC3]	0.5504	0.8453	0.6667	0.7635	0.6858	12
2	[PC1,PC7]	0.5178	0.8226	0.6356	0.7360	0.6716	11
3	[PC1,PC3,PC6,PC7,PC8]	0.5092	0.8377	0.6334	0.7420	0.6523	11

during the construction of the MST or the identification of the most central node; our method is unsupervised and does not require any training. As a result, the MST works with the whole sample at once, without the need to divide the sample into smaller pieces and risk losing relevant information in the process.

Table 1 shows that while rest-frame frequency width and brightness temperature demonstrated strong discriminatory power per se via median separation of the sample, the frequent occurrence of peak frequency in the selected combinations highlights its potential contribution to the classification process. This information can be valuable not only for optimizing the current method but also for informing feature selection strategies in other classification methods, for instance, using machine learning.

The performance of this method is on par or exceeds that of others. For instance, [Chen et al. \(2022\)](#); [Luo et al. \(2023\)](#); [Zhu-Ge et al. \(2023\)](#) use the sample from [CHIME/FRB Collaboration et al. \(2021\)](#) under a machine learning approach. We apply our methodology in the same conditions of [Luo et al. \(2023\)](#); [Zhu-Ge et al. \(2023\)](#), where the sample is composed of 594 FRBs, where 500 non-repeaters and 94 repeaters are noted. Under these assumptions, the results are a 97% recall

and an F_2 score of 77%, which is comparable to that obtained in the quoted papers. The recall is higher than those seen in [Chen et al. \(2022\)](#), where the sample is the same but they identify one repeater less (501 non-repeaters and 93 repeaters). In this work, the variable set adds more properties to deal with a total of 13 (10 observational and 3 model-dependent parameters, as they define), among which are several of those used in our set.

In Table 2 we show 33 currently labeled as non-repeaters FRBs that appear in the repeater branch identified using the 25 selected combinations obtained of variables showing a separating power exceeding a recall threshold of 82%. In the context of the MST strategy, these are strong candidates for repeating bursts. A few have been identified as well using machine learning methodologies in [Luo et al. \(2023\)](#); [Zhu-Ge et al. \(2023\)](#) Table 2 also shows the few FRBs denoted as outliers, those that are known repeaters but are consistently classified in the non-repeater branch of any of the 25 MSTs considered. Both candidates and outliers constitute a handle on the power and caveats of the technique, to keep an eye on with future samples of FRBs.

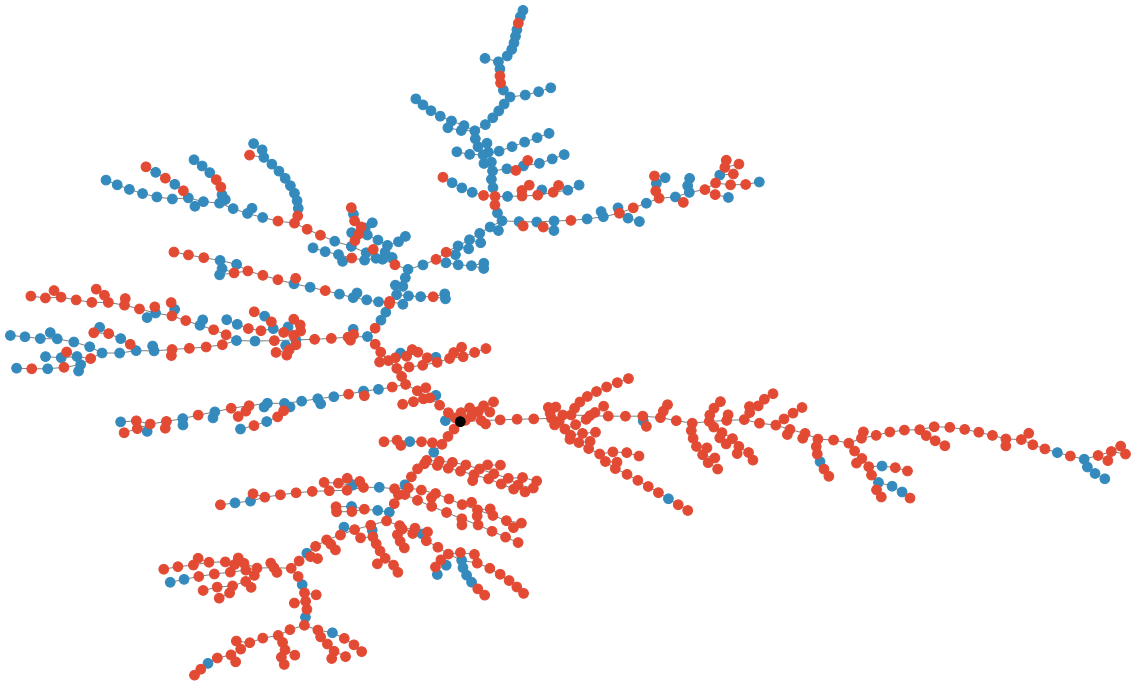


Figure 3. $T(750, 749)$ computed from the Euclidean distance based on the combination of peak frequency, rest-frame frequency width, and brightness temperature. Repeaters are shown in blue and non-repeaters in red. The most central node in terms of betweenness centrality appears in black.

Reducing false positives can be important to gain robustness, and attempts could be made to improve precision without significantly compromising recall. To refine the classification, a methodology that involves dividing the graph into significant branches (as introduced in García & Torres (2023)) could be of help.

Finally, one obvious enhancement we would like to perform provided the opportunity is to consider the rate of repetition of each of the repeating FRBs. In particular, we would like to see whether the MST grouping can distinguish a soft transition across the sample from the most commonly repeating FRBs to the non-repeater ones. However, this exercise is hindered by the current availability of data because such a rate should consider the right integration time for a particular field of view and this information is not provided in the catalog information CHIME/FRB Collaboration et al. (2021); The

Chime/FRB Collaboration et al. (2023). We encourage such data to be provided in future versions of the catalog, as it would be beneficial for this as well as similar analysis, and of course for comparing with any modeling of the repeating mechanism.

ACKNOWLEDGEMENTS

This work was supported by the grant PID2021-124581OB-I00 of MCIU/AEI/10.13039/501100011033 and 2021SGR00426. This work was also supported by the program Unidad de Excelencia María de Maeztu CEX2020-001058-M and by MCIU with funding from the European Union NextGeneration EU (PRTR-C17.I1). C. R. García thanks UNLV for its hospitality during part of this investigation.

REFERENCES

- Ai, S., Gao, H., & Zhang, B. 2021, ApJL, 906, L5
 Altmann, A., Tološi, L., Sander, O., & Lengauer, T. 2010, Bioinformatics, 26, 1340.
<https://doi.org/10.1093/bioinformatics/btq134>
 Baron, D., & Ménard, B. 2021, ApJ, 916, 91
 Beloborodov, A. M. 2017, ApJL, 843, L26
 Bhatporia, S., Walters, A., Murugan, J., & Weltman, A. 2023, arXiv e-prints, arXiv:2311.03456

Table 2. Properties of the currently labeled as non-repeater FRBs that are seen as repeaters for all combinations shown in Table 1. The 'Sub' column shows the sub-burst number to which each FRB corresponds. Candidate FRBs reported in Luo et al. (2023); Zhu-Ge et al. (2023) are highlighted in black. Repeaters not classified as such in any of the selected combinations (outliers) are shown below the line.

Name	Sub	RA (°)	Dec (°)	ν_c (MHz)	Δt_{BC} (ms)	S_ν (Jy)	F_ν (Jy ms)	z	$\Delta\nu$ (MHz)	Δt_r (ms)	E (erg)	L (erg/s)	T_B (K)
FRB20180907E	0	167.88	47.09	400.20	11.80	0.73	6.90	0.3118	178.54	3.16	7.11×10^{39}	9.87×10^{41}	7.74×10^{27}
FRB20180920B	0	191.09	63.52	421.10	10.81	0.35	1.70	0.4007	116.53	1.66	3.10×10^{39}	8.93×10^{41}	6.71×10^{27}
FRB20180928A	0	312.95	30.85	400.20	2.95	1.34	2.50	0.0022	92.11	0.27	1.20×10^{35}	6.44×10^{37}	1.06×10^{25}
FRB20181017B	0	237.76	78.50	593.20	12.78	1.06	6.50	0.2067	247.97	1.91	4.24×10^{39}	8.35×10^{41}	1.86×10^{27}
FRB20181022E	0	221.18	27.13	443.70	2.95	0.69	2.08	0.2073	193.28	0.33	1.02×10^{39}	4.09×10^{41}	4.09×10^{28}
FRB20181125A	0	147.94	33.93	434.50	14.75	0.39	3.20	0.1710	156.33	1.09	1.04×10^{39}	1.48×10^{41}	6.49×10^{26}
FRB20181125A	1	147.94	33.93	436.60	14.75	0.39	3.20	0.1710	177.76	1.23	1.04×10^{39}	1.49×10^{41}	6.43×10^{26}
FRB20181125A	2	147.94	33.93	426.50	14.75	0.39	3.20	0.1710	141.34	1.35	1.02×10^{39}	1.45×10^{41}	6.73×10^{26}
FRB20181214A	0	70.00	43.07	435.00	2.95	0.156	0.41	0.2308	116.19	0.43	2.47×10^{38}	1.15×10^{41}	1.20×10^{28}
FRB20181220A	0	346.11	48.43	400.20	2.95	1.33	3.00	0.0022	196.64	0.43	1.44×10^{35}	6.39×10^{37}	1.05×10^{25}
FRB20181226E	0	303.56	73.64	400.20	2.95	0.48	1.35	0.1779	186.23	0.99	4.37×10^{38}	1.83×10^{41}	2.55×10^{28}
FRB20181229B	0	238.37	19.78	445.50	20.64	0.42	4.90	0.3197	154.80	2.55	5.92×10^{39}	6.70×10^{41}	1.24×10^{27}
FRB20190112A	0	257.98	61.20	697.70	9.83	1.40	16.20	0.3476	317.48	1.22	3.64×10^{40}	4.24×10^{42}	8.80×10^{27}
FRB20190128C	0	69.80	78.94	491.60	15.73	0.71	5.90	0.1772	238.50	5.23	2.32×10^{39}	3.29×10^{41}	8.73×10^{26}
FRB20190206B	0	49.76	79.50	506.40	19.66	0.95	9.60	0.2190	350.34	5.82	6.03×10^{39}	7.27×10^{41}	1.09×10^{27}
FRB20190206A	0	244.85	9.36	534.50	5.90	1.40	9.10	0.0618	213.84	0.76	4.53×10^{38}	7.40×10^{40}	1.20×10^{27}
FRB20190218B	0	268.70	17.93	588.00	17.69	0.57	5.90	0.4416	334.17	1.42	1.84×10^{40}	2.56×10^{42}	2.56×10^{27}
FRB20190223A	0	64.72	87.65	444.80	3.93	0.47	1.58	0.2865	149.61	0.59	1.52×10^{39}	5.81×10^{41}	3.05×10^{28}
FRB20190308C	0	188.36	44.39	453.40	21.63	0.47	4.80	0.4542	218.85	0.28	1.22×10^{40}	1.74×10^{42}	2.51×10^{27}
FRB20190308C	1	188.36	44.39	449.00	21.63	0.47	4.80	0.4542	211.58	0.38	1.21×10^{40}	1.72×10^{42}	2.56×10^{27}
FRB20190323D	0	56.88	46.93	400.20	12.78	0.37	2.49	0.5930	204.86	3.41	9.66×10^{39}	2.29×10^{42}	1.26×10^{28}
FRB20190329A	0	65.54	73.63	432.30	11.80	0.52	2.24	0.0022	73.87	1.04	1.16×10^{35}	2.70×10^{37}	2.20×10^{23}
FRB20190410A	0	263.47	-2.37	515.70	6.88	1.59	5.80	0.0728	182.92	0.94	3.89×10^{38}	1.14×10^{41}	1.51×10^{27}
FRB20190412B	0	285.65	19.25	400.20	42.27	0.68	12.80	0.0146	228.59	6.70	2.60×10^{37}	1.40×10^{39}	1.11×10^{24}
FRB20190423B	0	298.58	26.19	537.60	9.83	0.87	7.00	0.0031	159.79	2.48	8.54×10^{35}	1.06×10^{38}	6.48×10^{23}
FRB20190423B	1	298.58	26.19	524.60	9.83	0.87	7.00	0.0031	148.96	8.47	8.33×10^{35}	1.04×10^{38}	6.81×10^{23}
FRB20190429B	0	329.93	3.96	422.40	16.71	0.74	5.00	0.1944	50.64	5.34	2.05×10^{39}	3.62×10^{41}	1.32×10^{27}
FRB20190430A	0	77.70	87.01	433.80	19.66	0.75	7.70	0.2278	214.13	2.75	4.50×10^{38}	5.38×10^{41}	1.27×10^{27}
FRB20190527A	0	12.45	7.99	484.70	57.02	0.47	10.10	0.5367	205.46	1.74	3.87×10^{40}	2.77×10^{42}	4.46×10^{26}
FRB20190527A	1	12.45	7.99	449.10	57.02	0.47	10.10	0.5367	172.11	1.61	3.59×10^{40}	2.56×10^{42}	5.20×10^{26}
FRB20190601C	0	88.52	28.47	517.00	5.90	1.32	5.80	0.1753	223.54	0.58	2.35×10^{39}	6.28×10^{41}	1.02×10^{28}
FRB20190601C	1	88.52	28.47	502.20	5.90	1.32	5.80	0.1753	201.91	0.43	2.28×10^{39}	6.10×10^{41}	1.08×10^{28}
FRB20190617B	0	56.43	1.16	459.30	13.76	0.99	9.20	0.1655	217.37	6.50	2.94×10^{39}	3.69×10^{41}	1.58×10^{27}
FRB20180910A	0	354.83	89.01	417.60	0.98	6.50	5.60	0.6230	649.22	0.126	2.51×10^{40}	4.73×10^{43}	3.82×10^{31}
FRB20190210C	0	313.90	89.19	448.50	1.97	2.37	3.60	0.5798	631.93	0.181	1.50×10^{40}	1.56×10^{43}	2.58×10^{30}
FRB20200726D	0	294.75	59.40	684.00	4.92	0.76	3.48	1.3812	541.72	0.407	1.23×10^{41}	6.37×10^{43}	3.17×10^{29}

Bochenek, C. D., Ravi, V., Belov, K. V., et al. 2020, Nature, 587, 59

Brandes, U. 2001, The Journal of Mathematical Sociology, 25, 163. <https://doi.org/10.1080/0022250X.2001.9990249>

Breiman, L. 2001, Machine Learning, 45, 5

Bruce, P., Bruce, A., & Gedeck, P. 2020, Practical statistics for data scientists: 50 essential concepts, 2nd edn. (O'Reilly Media)

Caleb, M., Stappers, B. W., Rajwade, K., & Flynn, C. 2019, MNRAS, 484, 5500

Casalichio, G., Molnar, C., & Bischl, B. 2018, arXiv e-prints, arXiv:1804.06620

Chen, B. H., Hashimoto, T., Goto, T., et al. 2022, MNRAS, 509, 1227

CHIME/FRB Collaboration, Andersen, B. C., Bandura, K. M., et al. 2020, Nature, 587, 54

CHIME/FRB Collaboration, Amiri, M., Andersen, B. C., et al. 2021, ApJS, 257, 59

Cordes, J. M., & Chatterjee, S. 2019, ARA&A, 57, 417

de Amorim, L. B. V., Cavalcanti, G. D. C., & Cruz, R. M. O. 2023, Applied Soft Computing, 133, 109924

Deng, W., & Zhang, B. 2014, ApJL, 783, L35

Erickson, J. 2019, Algorithms (Jeff Erickson, Lecture Notes University of Illinois at Urbana-Champaign)

Everitt, B., Landau, S., Leese, M., & Stahl, D. 2011, Cluster analysis, 5th edn. (Wiley)

Feng, Y., Li, D., Yang, Y.-P., et al. 2022, Science, 375, 1266

Fisher, A., Rudin, C., & Dominici, F. 2018, arXiv e-prints, arXiv:1801.01489

Freeman, L. C. 1977, Sociometry, 40, 35.

<http://www.jstor.org/stable/3033543>

García, C. R., & Torres, D. F. 2023, MNRAS, 520, 599

- García, C. R., Torres, D. F., & Patruno, A. 2022, *MNRAS*, 515, 3883
- Han, J., Kamber, M., & Pei, J. 2012, *Data Mining: Concepts and Techniques*, 3rd edn. (Morgan Kaufmann Publishers)
- Katz, J. I. 2016, *ApJ*, 826, 226
- . 2018, *Progress in Particle and Nuclear Physics*, 103, 1
- Kleinberg, J., & Tardos, E. 2005, *Algorithm design* (Addison Wesley)
- Kruskal, J. B. 1956, *Proc. Amer. Math. Soc.*, 7, 48
- Kumar, P., Lu, W., & Bhattacharya, M. 2017, *MNRAS*, 468, 2726
- Li, C. K., Lin, L., Xiong, S. L., et al. 2021, *Nature Astronomy*, 5, 378
- Li, X., Wang, X., & Xiao, G. 2017, *Briefings in Bioinformatics*, 20, 178.
<https://doi.org/10.1093/bib/bbx101>
- Lin, H.-H., Scholz, P., Ng, C., et al. 2023a, arXiv e-prints, arXiv:2307.05261
- . 2023b, arXiv e-prints, arXiv:2307.05262
- Lorimer, D. R., Bailes, M., McLaughlin, M. A., Narkevic, D. J., & Crawford, F. 2007, *Science*, 318, 777
- Lu, W., & Kumar, P. 2016, *MNRAS*, 461, L122
- Lu, W., Kumar, P., & Zhang, B. 2020, *MNRAS*, 498, 1397
- Lundberg, S., & Lee, S.-I. 2017, arXiv e-prints, arXiv:1705.07874
- Lundberg, S. M., Erion, G. G., & Lee, S.-I. 2018, arXiv e-prints, arXiv:1802.03888
- Luo, J.-W., Zhu-Ge, J.-M., & Zhang, B. 2023, *MNRAS*, 518, 1629
- Lyubarsky, Y. 2014, *MNRAS*, 442, L9
- Macquart, J. P., Prochaska, J. X., McQuinn, M., et al. 2020, *Nature*, 581, 391
- Margalit, B., & Metzger, B. D. 2018, *ApJL*, 868, L4
- Mereghetti, S., Savchenko, V., Ferrigno, C., et al. 2020, *ApJL*, 898, L29
- Metzger, B. D., Berger, E., & Margalit, B. 2017, *ApJ*, 841, 14
- Moxley, R. L., & Moxley, N. F. 1974, *Sociometry*, 37, 122.
<http://www.jstor.org/stable/2786472>
- Murase, K., Kashiyama, K., & Mészáros, P. 2016, *MNRAS*, 461, 1498
- Nicholl, M., Williams, P. K. G., Berger, E., et al. 2017, *ApJ*, 843, 84
- Palaniswamy, D., Li, Y., & Zhang, B. 2018, *ApJL*, 854, L12
- Pearson, K. 1901, *The London, Edinburgh, and Dublin Philosophical Magazine and Journal of Science*, 2, 559
- Petroff, E., Hessels, J. W. T., & Lorimer, D. R. 2019, *A&A Rv*, 27, 4
- . 2022, *A&A Rv*, 30, 2
- Platts, E., Weltman, A., Walters, A., et al. 2019, *PhR*, 821, 1
- Popov, S. B., & Postnov, K. A. 2013, arXiv e-prints, arXiv:1307.4924
- Popov, S. B., Postnov, K. A., & Pshirkov, M. S. 2018, *Physics Uspekhi*, 61, 965
- Scholz, P., Spitler, L. G., Hessels, J. W. T., et al. 2016, *ApJ*, 833, 177
- Shlens, J. 2014, arXiv e-prints, arXiv:1404.1100
- Spitler, L. G., Scholz, P., Hessels, J. W. T., et al. 2016, *Nature*, 531, 202
- The Chime/FRB Collaboration, Andersen, B. C., Bandura, K., et al. 2023, *ApJ*, 947, 83
- Vohl, D., van Leeuwen, J., & Maan, Y. 2023, arXiv e-prints, arXiv:2311.09201
- Wilson, R. J. 2010, *Introduction to graph theory* (Pearson)
- Xiao, D., Wang, F., & Dai, Z. 2021, *Science China Physics, Mechanics, and Astronomy*, 64, 249501
- . 2022, in *Handbook of X-ray and Gamma-ray Astrophysics*, 28
- Yang, Y.-P., & Zhang, B. 2021, *ApJ*, 919, 89
- Zhang, B. 2020, *Nature*, 587, 45
- . 2023, *Reviews of Modern Physics*, 95, 035005
- Zhu-Ge, J.-M., Luo, J.-W., & Zhang, B. 2023, *MNRAS*, 519, 1823

APPENDIX

Precision quantifies the ratio of repeaters that were correctly identified concerning the total in the branch, while *Recall* (also known as *sensitivity*) measures the proportion of actual repeaters that were correctly classified. The F measure, defined as

$$F_{\beta} = (1 + \beta^2) \frac{\text{Precision Recall}}{(\beta^2 \text{Precision}) + \text{Recall}} \quad (3)$$

evaluates the predictive performance by combining precision and recall through a weighted harmonic mean. The importance of precision ($\beta < 1$) versus recall ($\beta > 1$) is modulated by the β parameter. When $\beta = 1$, precision and recall are equally weighted. The F_1 score is obtained when $\beta = 1$, therefore leading to an equal emphasis on precision and recall. The F_2 score, alternatively, is derived when $\beta = 2$, giving more importance to recall over precision. The *Receiver Operating Characteristic (ROC)* curve is a graphical representation of the performance of a binary classification model across different threshold settings. It plots the true positive rate (sensitivity) against the false positive rate (1 - specificity) at various threshold values. Here, *Specificity*, also known as the true negative rate, measures the proportion of actual negative instances (non-repeater FRBs) correctly identified as negative. The ROC curve helps assess the trade-off between sensitivity and specificity and provides insights into the classifier's ability to discriminate between positive and negative instances. The *Area Under the Curve (AUC)* value quantifies the overall performance of a binary classification model represented by the ROC curve. It measures the area under the ROC curve, with values ranging from 0 to 1. AUC values closer to 1 indicate better discrimination ability of the classifier, while values closer to 0.5 suggest poor discrimination (similar to random guessing).

The labels assigned to repeaters and non-repeaters according to the repeater branch are as follows:

- **True Positive (TP)**: Repeaters correctly classified as repeaters
- **False Positive (FP)**: Non-repeaters incorrectly classified as repeaters.
- **True Negative (TN)**: Non-repeaters correctly classified as non-repeaters.
- **False Negative (FN)**: Repeaters incorrectly classified as non-repeaters.

with these, the scores are defined as

$$\text{Precision} = \frac{TP}{TP + FP} \quad (4)$$

$$\text{Recall} = \frac{TP}{TP + FN} \quad (5)$$

$$\text{Specificity} = \frac{TN}{TN + FP} \quad (6)$$

$$F_1 \text{ Score} = \frac{2 \text{ Precision Recall}}{\text{Precision} + \text{Recall}} \quad (7)$$

$$F_2 \text{ Score} = \frac{5 \text{ Precision Recall}}{4 \text{ Precision} + \text{Recall}} \quad (8)$$

The Z-score, also known as the standard score or z-value, is a statistical measure that quantifies how many standard deviations a data point is from the mean of a dataset. It is defined as

$$Z = \frac{x - \mu}{\sigma}. \quad (9)$$

Here x is the value of the data point (the classifier's recall), μ and σ are the mean and the standard deviation of the dataset (distribution from the fake cases), respectively. A Z-score of 0 indicates that the data point is exactly at the mean of the dataset, while positive and negative Z-scores indicate that the data point is above and below the mean, respectively. A Z-score higher than 2σ or 3σ in absolute value is significant at the 5% or even 1% level.